THE AMERICAN SOCIETY OF MECHANICAL ENGINEERS
345 E. 47 St., New York, N.Y. 10017

The Society shall not be responsible for statements or opinions advanced in papers or in discussion at meetings of the Society or of its Divisions or Sections, or printed in its publications. Discussion is printed only if the paper is published in an ASME Journal. Papers are available from ASME for fifteen months after the meeting.
Printed in USA.

Copyright © 1986 by ASME

86-GT-271

Check for updates

The Effect of Reynolds Number and Velocity Distribution on LP Turbine Cascade Performance

D. J. PATTERSON
Turbine Technology Department,
Rolls-Royce Limited,
Bristol, U.K.

M. HOEGER
Institute for Design Aerodynamics,
DFVLR, Flughaven,
D3300 Braunschweig,
W. Germany.

ABSTRACT

Because of the laminar boundary-layer's inability to withstand moderate adverse pressure gradients without separating, profile losses in LP turbines operating at low Reynolds numbers can be high. The choice of design pressure distribution for the blading is thus of great importance.

Three sub-sonic LP turbine nozzle-guide-vane cascade profiles have been tested over a wide range of incidence, Mach number and Reynolds number. The three profiles are of low, medium and high deflection and, as such, display significantly different pressure distributions. The tests include detailed boundary-layer traverses, trailing-edge base-pressure monitoring and oil-flow visualisation.

It is shown that the loss variation with Reynolds number is a function of pressure distribution and that the trailing-edge loss component is dominant at low Reynolds number. The importance of achieving late flow transition - rather than separation - in the suction-surface trailing-edge region is stressed.

The paper concludes by remarking on the advantages and practical implications of each loading design.

NOMENCLATURE

a_0 = stagnation speed of sound

C = chord
C_p = pressure coefficient $(p-p_k)/(p_{t1}-p_k)$

$M_{2,is}$ = isentropic exit Mach number $(p_t=p_{t1}, p=p_k)$

p, p_t = static, total pressure

Q = U/a_0 (Crocco number)

Re_2 = isentropic exit Reynolds number
s = blade spacing

S, S_0 = surface length, total surface length

s^* = surface length ratio S/S_0
te = trailing-edge thickness

Tu = inlet turbulence level $(100\sqrt{\bar{u}_1^2})/u_1$
U,u = velocity
ΔU_{w12} = change in tangential velocity

x,z = rectangular coordinates, bi-tangential system

$\beta, \Delta\beta$ = flow angle, gas deflection
δ = boundary layer thickness
Γ = circulation $s.\Delta U_{w12}$

δ^* = Displacement thickness

$$\int_0^\delta \left(\frac{\rho_p(\eta) U_p(\eta)}{\rho_{pw} U_{pw}} - \frac{\rho(\eta) U(\eta)}{\rho_{pw} U_{pw}} \right) d\eta$$

θ = Momentum thickness

$$\int_0^\delta \frac{\rho(\eta) U(\eta)}{\rho_{pw} U_{pw}} \left(\frac{U_p(\eta)}{U_{pw}} - \frac{U(\eta)}{U_{pw}} \right) d\eta$$

ε = Energy thickness

$$\int_0^\delta \frac{\rho(\eta) U(\eta)}{\rho_{pw} U_{pw}} \left(\frac{U_p^2(\eta)}{U_{pw}^2} - \frac{U^2(\eta)}{U_{pw}^2} \right) d\eta$$

H_{12} = Shape parameter δ^*/θ

η = Distance normal to surface

Presented at the International Gas Turbine Conference and Exhibit
Dusseldorf, West Germany—June 8-12, 1986

Downloaded from http://asmedigitalcollection.asme.org/GT/proceedings-pdf/GT1986/79283/V001T01A113/2396540/v001t01a113-86-gt-271.pdf by guest on 16 August 2022

ζ_{V2} = Measured profile loss coefficient

$$\frac{p_{t1} - p_{t2}}{p_{t1} - p_2}$$

ρ = Density

Subscripts

1,2 = Up and downstream of the cascade
AX = Engine axis direction
P,PS = Pressure surface
S,SS = Suction surface
∞ = Edge of boundary layer
k = Wind-tunnel chamber
te = Trailing-edge
p = Frictionless flow
$p_t = p_{t\infty}$, $p = p(\eta)$
pw = Frictionless flow
$p_t = p_{t\infty}$, $p = p_{wall}$ ($\eta = 0$)

INTRODUCTION

As long as the turbo-fan engine fulfils its role in the civil and military fields, LP turbine efficiency will have a very noticeable influence on overall fuel consumption and engine performance. In a world where small improvements in cycle efficiency represent large savings in civil operators costs, or enhanced military flight performance, the quest for improved aerodynamic component efficiencies will always be an essential part of gas turbine design.

Two-dimensional aerodynamic cascade testing is a valuable technique for demonstrating the advantages of various turbine profile designs, and for detailed examination of certain loss mechanisms. Therefore, as a precursor to a full-scale, sub-sonic LP turbine design, three 2-D cascade profiles were designed and manufactured for testing in the High Speed Cascade Wind Tunnel, DFVLR, Braunschweig.

BACKGROUND

The two important flow parameters associated with gas turbine aerodynamic design are Mach and Reynolds number (Re). In the HP turbine, gas density is high and aerofoil chords have to be sufficiently large to accommodate air cooling. This usually results in high Re ($\geq 10^6$), and the resulting profile losses arise from an interaction of compressibility and viscosity effects.

With few exceptions, LP turbines operate at substantially lower Mach no. and Re because of prior expansion through the HP turbine. When a number of stages comprise the complete LP turbine, the subsequent stage expansions progressively reduce the operating pressure to well below that of the HP turbine. The operating pressure falls even further when the engine is operating at altitude. Since aerofoil Re is directly proportional to pressure level and scale, many current LP turbine blade rows operate at low Re ($10^4 \leq$ Re $\leq 5 \times 10^5$). At such values of Re, profile losses can be extremely high. It is

cascade	$\Delta\beta$ [°]	s/c
T9	18°	0.7952
T10	118°	0.7370
T11	68°	0.8175

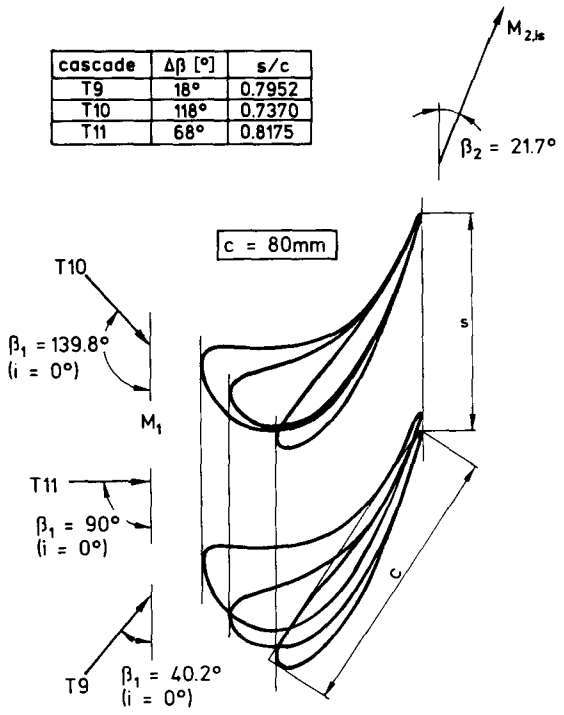

FIG. 1 CASCADE GEOMETRIES

in this flow regime where viscous effects are probably more significant than those of compressibility, and the aerodynamicist needs to be aware of the risks involved in opting for certain aerofoil designs.

At 'high' Re ($> 10^6$), aerofoil boundary layers possess high inertial energy and an ability to withstand quite large adverse pressure gradients without separating from the surface. The phenomenon of boundary layer transition from the laminar to turbulent regime tends to occur quite rapidly and naturally (i.e. without need of any flow disturbance), and profile losses will rise due to longer turbulent lengths arising from early transition (1). At moderate Re (5×10^5 say), natural transition still occurs, but is considerably delayed. The boundary layer may well go into separation-initiated transition through the mechanism of the separation-bubble (2,3).

When Re drops to values of 1×10^5 (say) and below, boundary layer growth will initially be laminar. However, because viscous forces now dominate, flow separation occurs in regions of quite modest adverse pressure gradient. Characteristically, such an event is accompanied by a sharp increase in profile loss.

Since such characteristic low Re behaviour is initiated by pressure gradient, LP turbine aerofoil design pressure distribution is of fundamental importance.

PROFILE DESIGNS

The cascade profiles are representative of mid-streamline sections for three alternative stage 1 LP nozzle guide vanes. These vanes

Downloaded from http://asmedigitalcollection.asme.org/GT/proceedings-pdf/GT1986/79283/V001T01A113/2396540/v001t01a113-86-gt-271.pdf by guest on 16 August 2022

cascade	symb.	Δβ [°]	loading	s/c
T9	—·—	18°	comb.	0.7952
T10	- - - -	118°	aft	0.7370
T11	———	68°	mid	0.8175

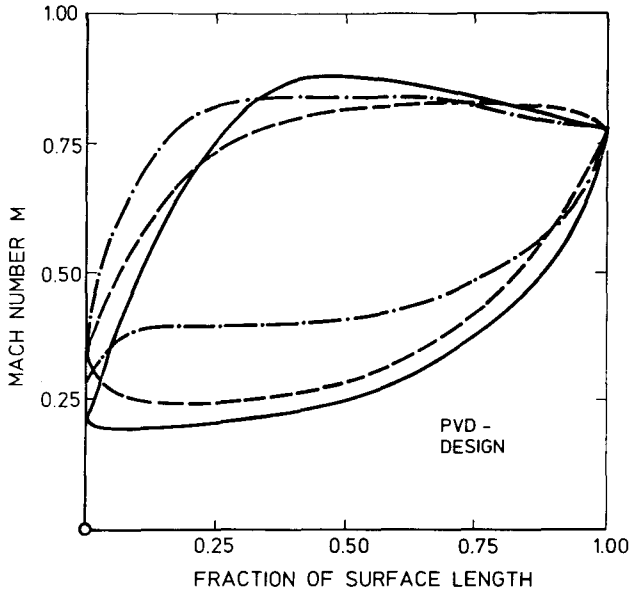

FIG. 2 DESIGN VELOCITY DISTRIBUTIONS

are designed for specific engine configurations in which

i) the HP and LP shafts either co or contra rotate, and
ii) the LP1 vane serves as bearing support strut and accommodates a lubrication service pipe.

The entry conditions to the LP1 rotor are fixed, and so to meet the above requirements, the three profiles have been designed for low, medium and high deflection while maintaining a suitable thickness for the lubrication service pipe.

The three profiles are designated:

T9 (low deflection - for contra-rotation),

T10 (high deflection - for co-rotation)

and T11 (medium deflection - for co/contra-rotation).

Both T9 and T11 profiles were designed to fit within the engine axial chord limitation as well as observing the maximum thickness requirement. Since pitch/chord and thickness/chord ratios are characteristically related to deflection (see Appendix), profile T10 was scaled-down to reduce the maximum thickness to the required value, allowing for reduced axial chord.

All three profile shapes were generated using a Prescribed Velocity Distribution (PVD) technique (see Fig. 1). The design velocity distributions are shown in Fig. 2. These are based on surface length such that real pressure gradients are represented.

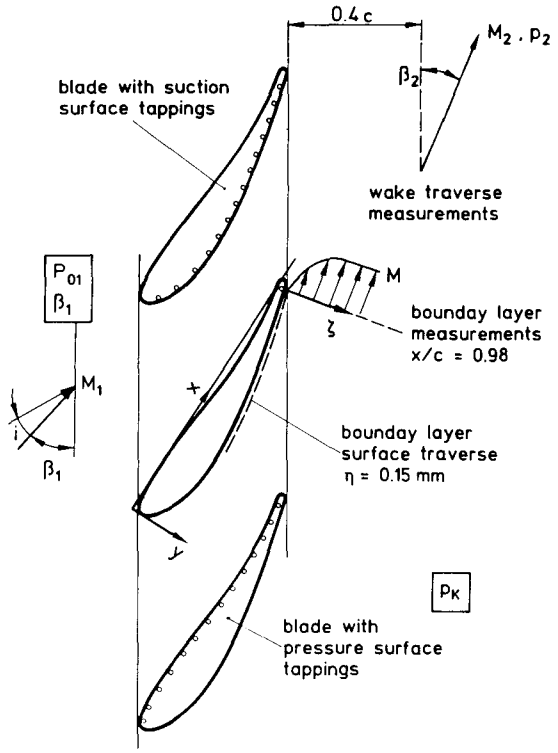

FIG.3 MEASUREMENT POSITIONS

AEROFOIL LOADING DEFINITIONS

'Loading' is a term relating an aerofoil's peak Mach number to some chord-wise or surface length parameter. Because the term is used to generally describe the position where suction-surface acceleration ends (or where diffusion starts), it is important that a universally recognised characteristic length parameter is used to avoid confusion. True or axial chord are geometrical parameters that have no direct relevance to surface length, which is a true characteristic of the flow regime. Aerofoil loading defined on a chord-wise basis does not intimate the levels and regions of pressure gradient since these change with deflection. Surface length is therefore adopted to describe the loading of profiles T9, T10 and T11, since the effect of true pressure gradient is under scrutiny.

Profile T9 will be referred to as 'combination' loaded, since acceleration ends forward, but the diffusion starts aft - by virtue of a constant velocity region. Forward/combination loading is typical of low deflection vanes.

Profile T10 is aft loaded, T11 is mid loaded.

Both of these latter distributions are typical of general LP blades and vanes.

INSTRUMENTATION AND PROCEDURE

The experimental investigations were performed in the High Speed Cascade Wind Tunnel of the DFVLR - Braunschweig (4). Mach and Reynolds number were varied independently.

The cascades were of seven or nine blades with true chord of 80 mm. With a high aspect

Downloaded from http://asmedigitalcollection.asme.org/GT/proceedings-pdf/GT1986/79283/V001T01A113/2396540/v001t01a113-86-gt-271.pdf by guest on 16 August 2022

ratio (H/C) of 3,75, the mid section of each cascade tends to show two-dimensional flow. To avoid disturbances, pressure tappings were situated on two profiles neighbouring the test blade. The blade for wake traverse and boundary layer measurement had only a reference tapping near the trailing-edge suction surface, where boundary layer measurements were made (Fig. 3).

Wake traverse measurements were performed with a wedge probe (4) at an axial distance of 40% chord downstream of the cascade trailing-edge plane (Fig. 3). The measured flow quantities were converted to those of an equivalent homogeneous flow by applying the laws of conservation.

A two-finger boundary-layer probe was used to determine both total and static pressures within the boundary layer. The external height (h) of the flattened pitot tip was 0,15 mm. This probe was calibrated over a wide range of Mach and Reynolds numbers (5). Integral values were evaluated with variations in static pressure - as proposed by KIOCK (6). Values between the near-wall probe measurement and actually at the wall were linearly interpolated.

Another flattened pitot probe (h = 0.3 mm) was moved along the surface from approximately 50% to 98% chord to detect separation and/or transition zones (Fig. 4). To supplement the pitot traverse results, oil-dye flow visualisation was made.

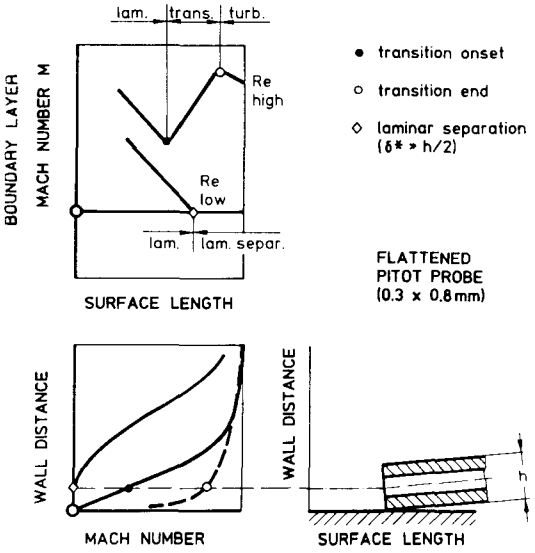

FIG.4 DEFINITION OF TRANSITION & SEPARATION POINTS FROM PITOT SURFACE MEASUREMENTS

To simulate engine-like flow conditions, the inlet turbulence intensity (Tu) was increased artificially to approximately 4%.

The aerodynamic behaviour of the three cascades was investigated over a wide range of sub-sonic exit Mach numbers, incidence and Reynolds number. Boundary-layer and loss data are presented for the effect of Re variation ($10^5 \leq Re_2 \leq 10^6$) only. Mach no. and incidence were held at their design conditions (0.78 and zero, respectively). Variation in

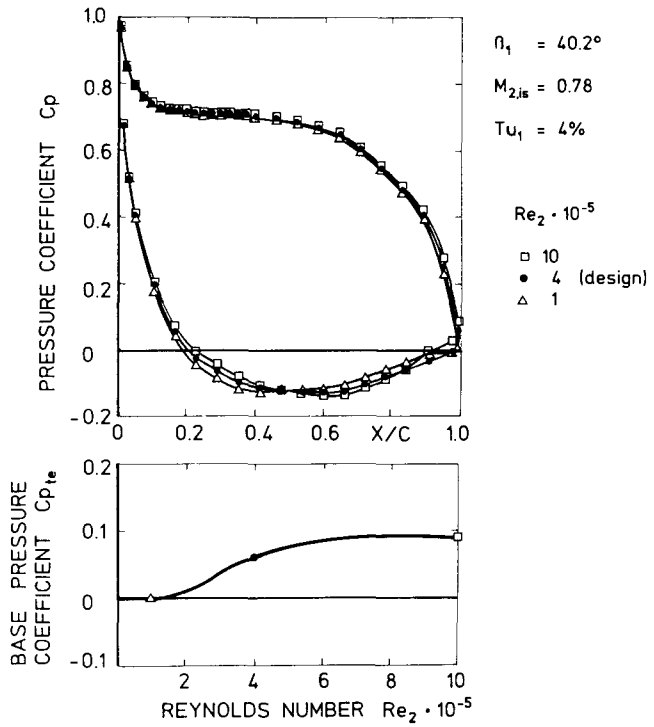

FIG.5 PRESSURE DISTRIBUTIONS OF COMBINATION -LOADED CASCADE T9

exit angle is not discussed.

Boundary layer development on the suction side (only) of each cascade is shown qualitatively from pressure distributions, oil flow patterns and pitot traverses.

Results are displayed against true chord position (x/l) unless stated otherwise.

MEASURED DATA

The measured pressure distributions for the combination loaded cascade T9 are shown in Fig. 5. For high Re_2 ($\longrightarrow 10^6$), the pressure distribution approaches that of potential flow. With decreasing Re_2 the boundary layers develop and cause changes in the pressure distribution, although positive base pressures occur. At $Re_2 = 10^5$ an inflection point near x/l = 0.85 on the suction side suggests that separation has taken place, causing low base pressure coefficients (Cpte$\longrightarrow$0.). The boundary layer then interacts with the undisturbed flow and causes the point of minimum pressure to shift upstream and the rate of diffusion to decrease as Re_2 falls. Measured suction surface boundary layer velocity profiles (98% chord) and the corresponding integral values are shown in Figs. 6 and 7 respectively.

Regions of differing boundary layer conditions are presented in Fig. 8, together with measured profile Mach number distributions. Transition starts for high Re2 (10^6) at approximately 85% chord. With falling Re2, the point of transition onset is indicated further downstream, nearer 90% chord. A further reduction of Re2 then causes the boundary layer to separate at about 80%

Downloaded from http://asmedigitalcollection.asme.org/GT/proceedings-pdf/GT1986/79283/V001T01A113/2396540/v001t01a113-86-gt-271.pdf by guest on 16 August 2022

chord. (It will be shown later, that the separation zone itself is not the significant parameter in the development of the profile losses at low Re2.). A comparison of the suction-side design (PVD) Mach number distribution, with that measured (Fig. 8), shows good agreement even for Re2 = 10^5 and with separated flow. The displacement effect of the boundary layer is therefore small.

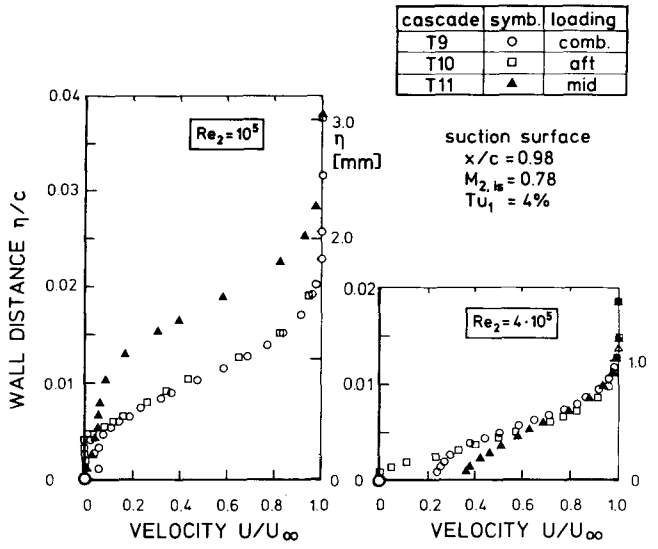

FIG.6 COMPARISON OF BOUNDARY LAYER VELOCITY PROFILES AT 98% CHORD ON SUCTION SURFACE

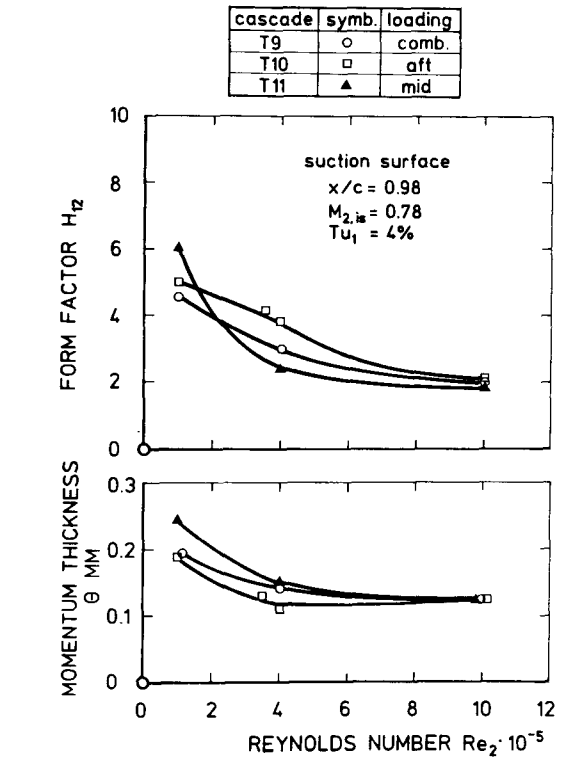

FIG.7 COMPARISON OF INTEGRAL VALUES AT 98% CHORD ON SUCTION SURFACE

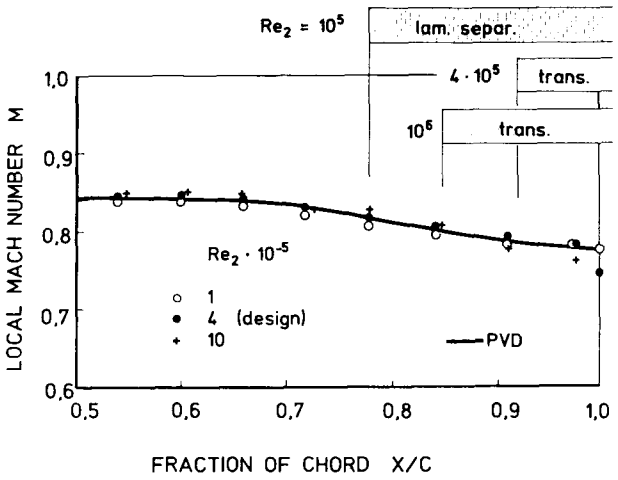

FIG.8 SURFACE MACH NO. DISTRIBUTIONS & TRANSITION/SEPARATION ZONES FOR COMBINATION-LOADED CASCADE T9

Pressure distributions for the aft-loaded cascade (Fig. 9), show a long region of accelerated flow, followed by a short region of diffusion. Boundary layer investigation showed completely different behaviour from that of the combination loaded profile. Over the range $10^5 \leqslant Re2 \leqslant 10^6$, low base pressures (Fig. 9) coincide with a flattening of the pressure distribution in the suction-surface trailing-edge region (Fig. 10). At high Re2 (10^6), suction-side transition onset is indicated after 90% chord. At 98% chord, a

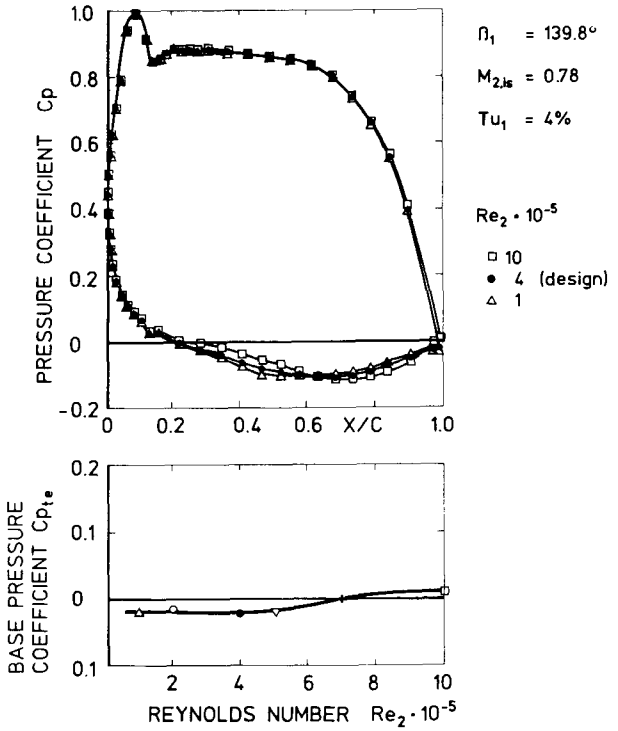

FIG.9 PRESSURE DISTRIBUTIONS FOR AFT-LOADED CASCADE T10

Downloaded from http://asmedigitalcollection.asme.org/GT/proceedings-pdf/GT1986/79283/V001T01A113/2396540/v001t01a113-86-gt-271.pdf by guest on 16 August 2022

transitional boundary layer was observed. Separation of the transitional boundary layer is suspected to occur extremely close to the trailing-edge, since extremely small, positive base pressures were observed.

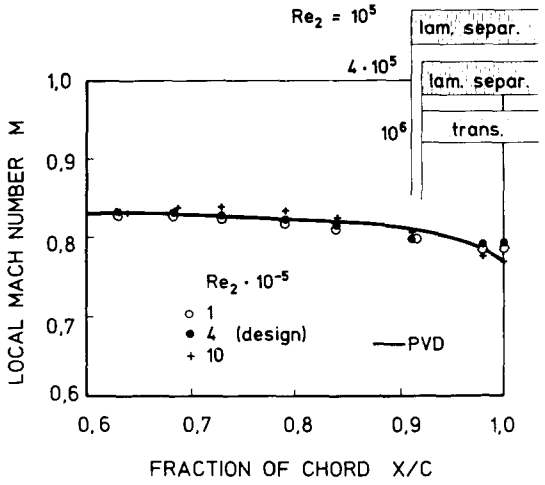

FIG.10 SURFACE MACH NO. DISTRIBUTIONS & TRANSITION/SEPARATION ZONES FOR AFT-LOADED CASCADE T10

Reducing Re ($\lesssim 4 \times 10^5$) causes separation to occur further upstream of the trailing-edge (Fig. 10), thus avoiding transition altogether. It was noted that the aft-loaded design delayed transition and allowed for a mainly laminar suction surface boundary layer. This produced very low momentum thickness, even for $4 \times 10^5 \lesssim Re_2 \lesssim 1 \times 10^6$ (Fig. 7). This suggests that aft-loading tends to reduce friction losses.

In order to confirm the presence of small areas of detached flow, flow visualisation was performed. The oil flow-pattern in Fig. 11 shows (for $Re_2 = 4 \times 10^5$) an accumulation of dye in the region of diminishing shear stress, near the separation point (light area in photographs). (N.B. The height of the separation bubble is smaller than the flattened pitot-probe (external height .3 mm), which considerably reduces accuracy under these conditions. Similar observations are made in (7). Only at lower Re2, and with comparitively thicker boundary-layers, do the two techniques concur.).

Pressure distributions and base pressure coefficients for the mid-loaded cascade (T11) are given in Fig. 12. When Re2 is sufficiently high, a transitional boundary layer enters the suction-side trailing-edge region allowing for high base pressures. A reduction of the Reynolds number moves the point of transition downstream and produces (for $Re2 = 4.10^5$) a small separation bubble. Transition then takes place in the highly unstable free shear layer some distance from the profile surface, followed by re-attachment caused by the entrainment of high energy fluid (2). Such a so-called laminar separation bubble can be observed as a small distortion in the pressure distribution and was seen by oil flow visualisation (Fig. 13). Re-attachment is indicated for the design Re2 (4.10^5) by the grainy structure in the oil flow pattern near 95% chord. At $Re2 = 4 \times 10^5$, a transitional boundary layer is indicated which, at 98% chord, has H_{12} near 2.5 (Fig. 7). When the re-attachment point of the bubble leaves the surface, a sharp increase in H_{12} (>5) occurs. Again, pitot traversing was unable to resolve the thin local separation zone, but indicated increasing velocities at 92% chord. This was slightly upstream of the re-attachment point suggested by the flow visualisation study.

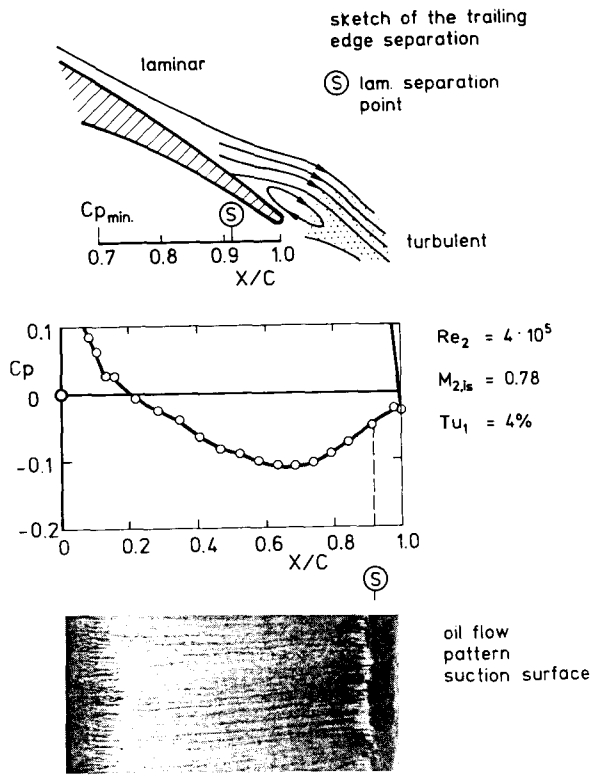

FIG.11 COMPARISON OF PRESSURE DISTRIBUTION WITH FLOW VISUALISATION. AFT-LOADED CASCADE T10

With falling Re2, the length of the laminar separation bubble increases. The rapid change from positive to negative base pressure coefficient (Fig. 12) for $Re2 \lesssim 3.10^5$ indicates that the re-attachment point has left the surface. Although the suction-side boundary layer is now fully separated, changing the pressure distribution completely, the position of the separation point is found to be nearly the same at about 80% chord for $Re2 = 10^5$ and 4.10^5 (Fig. 14). (3) gives similar findings.

At $Re2 = 1 \times 10^5$, the displacement effect in the trailing-edge region is the largest of all three designs. This is because the long region of adverse pressure gradient promotes early separation at 80% chord.

CALCULATED PROFILE LOSSES FROM BOUNDARY LAYER DATA

To gain insight into the various loss

Downloaded from http://asmedigitalcollection.asme.org/GT/proceedings-pdf/GT1986/79283/V001T01A113/2396540/v001t01a113-86-gt-271.pdf by guest on 16 August 2022

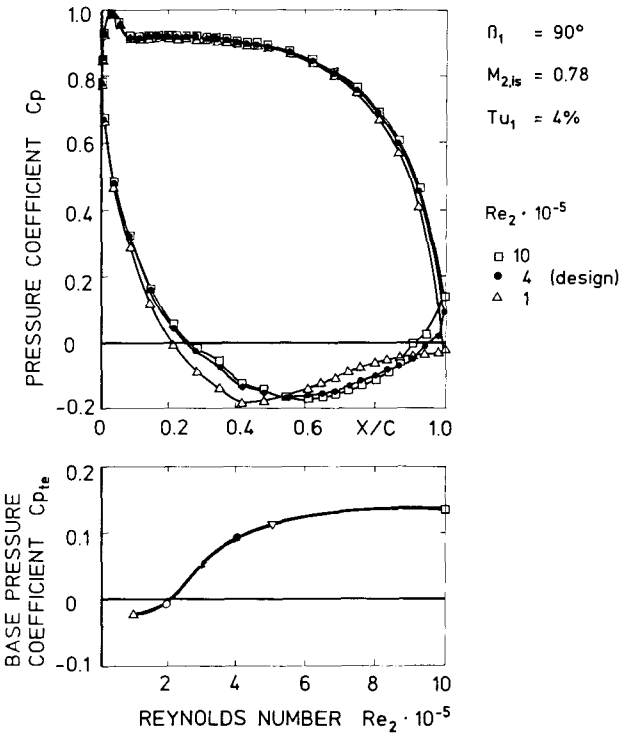

FIG.12 PRESSURE DISTRIBUTIONS FOR MID-LOADED CASCADE T11

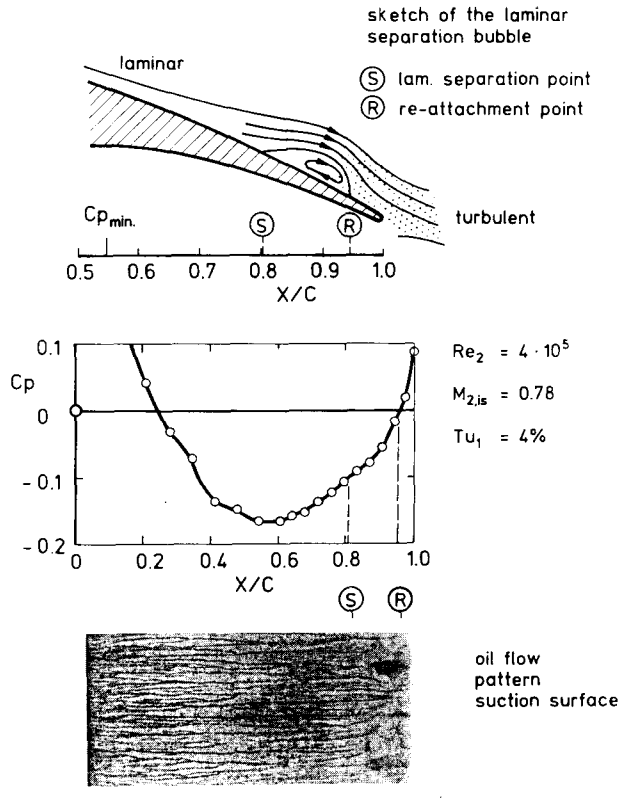

FIG.13 COMPARISON OF PRESSURE DISTRIBUTION WITH FLOW VISUALISATION. MID-LOADED CASCADE T11

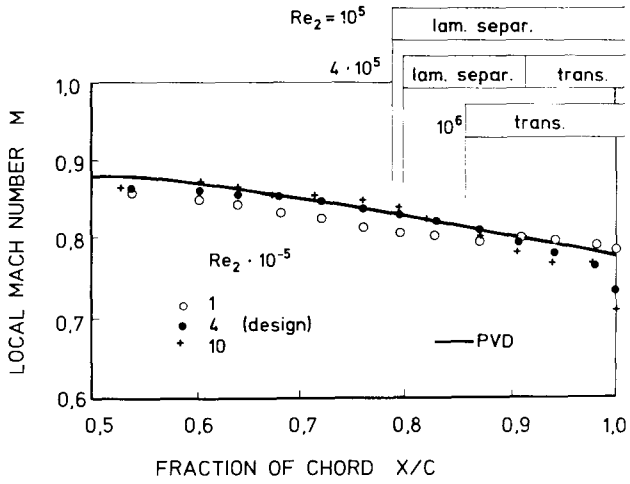

FIG.14 SURFACE MACH NO. DISTRIBUTIONS & TRANSITION/SEPARATION ZONES FOR MID-LOADED CASCADE T11

mechanisms involved, a comparison of the measured loss coefficient (ζ_{V2}) with a predicted loss coefficient (ζ_R - calculated from measured/theoretical trailing-edge boundary layer data) is made.

In linking a certain trailing-edge boundary layer state with the corresponding profile loss, the flow properties in the trailing-edge plane may be homogenised by applying the laws of conservation in the axial and tangential directions. Assuming the potential flow exit angle is not affected by the boundary layer displacement, loss coefficients (ζ_R) and equivalent boundary layer integral values may be calculated by the derivations given in (8) for two dimensional, incompressible flow:-

$$\zeta_R = \frac{P_{t1} - P_{t2}}{\frac{1}{2}\rho U_{2,is}^2} = \frac{2.\theta^*}{1 - 2.7\Delta^*} \quad (1)$$

$$\text{where } \theta^* = \frac{\bar{\theta}_{ss} + \bar{\theta}_{ps}}{s.\sin\beta_{2,is}} \quad (2)$$

$$\Delta^* = \frac{\bar{\delta}^*_{ss} + \bar{\delta}^*_{ps} + te}{s.\sin\beta_{2,is}} \quad (3)$$

$$\text{and } \frac{\bar{\delta}^*_\alpha}{\delta^*_\alpha} = \frac{\bar{\theta}_\alpha}{\theta_\alpha} = \frac{\bar{\varepsilon}_\alpha}{\varepsilon_\alpha} = \left[\frac{U_{\infty,\alpha}}{U_{2,is}}(1-\Delta^*)\right]^3 \quad (4)$$

($\delta^*_\alpha, \theta_\alpha, \varepsilon_\alpha$ - measured values

$\bar{\delta}^*_\alpha, \bar{\theta}_\alpha, \bar{\varepsilon}_\alpha$ - homogenised values)

Downloaded from http://asmedigitalcollection.asme.org/GT/proceedings-pdf/GT1986/79283/V001T01A113/2396540/v001t01a113-86-gt-271.pdf by guest on 16 August 2022

The influence of a finite trailing-edge thickness is included in equation (3) by assuming a "dead air" region of dimension te. Equation (1) contains the losses from friction on the blade surfaces and mixing of the non-homogeneous flow. For the derivation of equation (1), steady flow and uniform distribution of static pressure and flow angle was assumed. If separation occurs, boundary layer flow may become unsteady under the influence of shed vortices. These will cause pressure fluctuations (i.e. additional body forces) and high shear stresses, which are not taken into account in equation (1). It is supposed in (9) that Karman vortex streets are "the more important mechanism for lateral transport of axial momentum in the near-wake region than turbulence." When separation occurs, it is erroneous to assume that the average momentum in the cascade exit plane can be determined by boundary layer integral values alone. Such an assumption leads to an underestimate of profile loss.

For the evaluation of profile loss from boundary layer quantities, measured compressible integral values were used for the suction-surface at 98% chord. Energy dissipation downstream of the trailing-edge was therefore omitted. For the pressure-surface, predicted values from a finite-difference boundary layer calculation (similar to (10)) were obtained. The limitations of the coding do not significantly affect the predictions.

(The effect of compressibility on equations (1) to (4) amounts to approximately 15% on predicted loss, and was ignored).

COMPOSITION OF PROFILE LOSS

A comparison of the measured profile losses (ζ_{V2}) with the corresponding predicted values (ζ_R) is presented in Fig. 15. This highlights several important features. The predicted loss coefficients ζ_R lie, for all designs and Re2, in a band and approach the measured losses at high Re2 (10^6) and non-separated flow. At low Re2, boundary layer separation occurs, and the measured profile losses differ considerably from those predicted. If the integral values are believed, it is clear that loss mechanisms other than those accounted for in equation (1) influence the cascade behaviour to a large extent.

A trailing-edge loss coefficient ζ_{te} can be defined as:

$$\zeta_{te} = \zeta_{V2} - \zeta_{R\ (te\ =\ 0)} \qquad (5)$$

which gives a quantitative indication of the non-friction components of measured loss. Such values are plotted in the upper portion of Fig. 16. It is apparent that the three designs have unique 'effective' trailing-edge loss characteristics:

i) The aft-loaded profile has high effective trailing-edge loss even at high Re2 (10^6). This is due to the transitional suction-surface boundary layer separating at the trailing-edge. This will lead to an increase in 'effective' trailing-edge thickness and low base-pressures.

ii) The combination loaded profile has the lowest effective trailing-edge loss, and is some 40% better than the aft loaded profile at Re2 = 1 x 10^5.

iii) The mid-loaded profile has a characteristic mid-way between the previous two. Its best operating point is at high Re2.

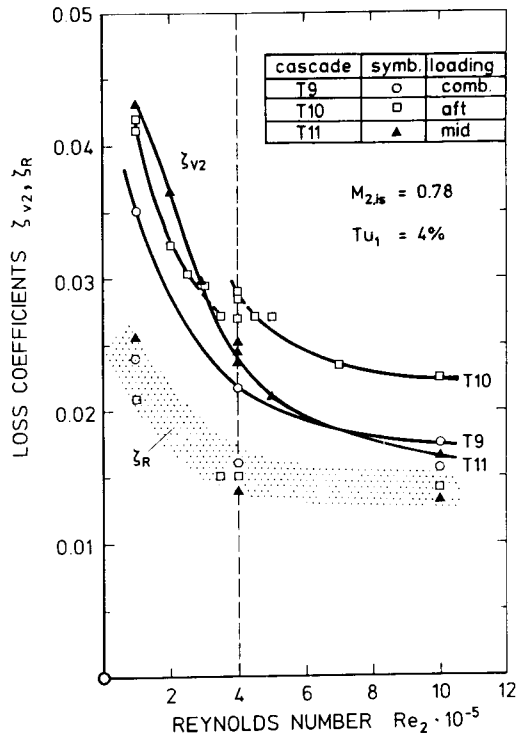

FIG. 15 COMPARISON OF MEASURED LOSS COEFFICIENT (ζ_{V2}) WITH THOSE PREDICTED (ζ_R) USING BOUNDARY LAYER DATA

If ζ_{V2} is replaced by ζ_R in equation (5), the trailing-edge loss coefficient ζ_{te} becomes:

$$\zeta'_{te} = \zeta_R - \zeta_{R\ (te\ =\ 0)} \qquad (6)$$

where ζ'_{te} ignores downstream energy dissipation (Fig. 16). At high Re2, the mid and combination-loaded profiles have ζ_{te} values that compare well with ζ'_{te} and also with an empirical expression given by DENTON (11).

At low Re2, viscous forces and unsteady separations begin to dominate all three designs. Comparison of the ζ_{te} and ζ'_{te} curves in Fig. 16 then shows that the mathematical model used to derive equation (1) is inadequate when separations begin to occur in the trailing-edge region. It also shows that

Downloaded from http://asmedigitalcollection.asme.org/GT/proceedings-pdf/GT1986/79283/V001T01A113/2396540/v001t01a113-86-gt-271.pdf by guest on 16 August 2022

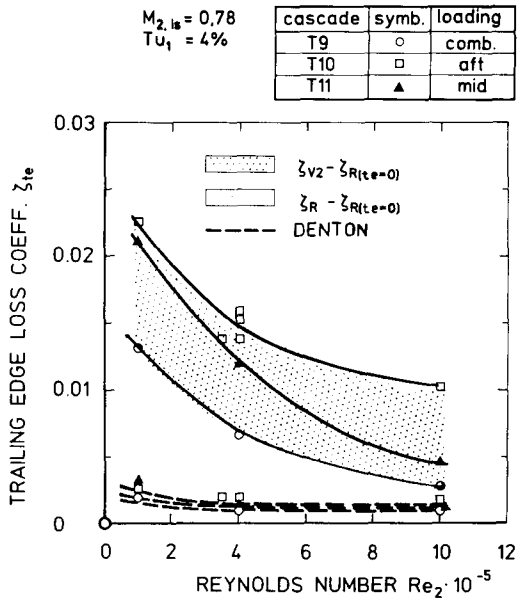

FIG. 16 COMPARISON OF TRAILING-EDGE LOSS COEFFICIENTS (ζ) FROM MEASUREMENT AND PREDICTION

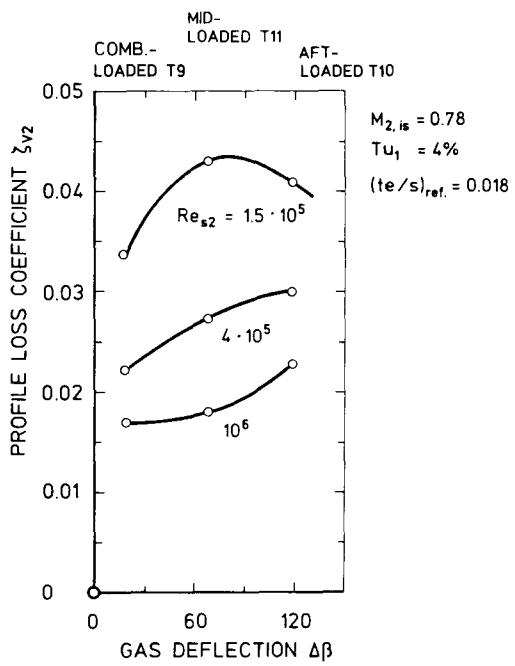

FIG. 17 MEASURED PROFILE LOSS COEFFICIENTS (ζ_{V2}) FOR REYNOLDS NO. BASED ON SUCTION -SURFACE LENGTH

effective trailing-edge loss rapidly grows in importance over friction loss at low Re2.

(9) discusses how the base-pressure is influenced by unsteady vortex shedding on a trailing-edge with zero diffusion. The separating cascade boundary layer tends to adjust itself by accelerating the mainstream flow and thus reduces the suction-side diffusion. A small amount of diffusion is shifted into the wake, causing negative base pressures and so-called Form Drag. This body force and dissipation are thought to be linked to complicated unsteady wake mixing, and high trailing-edge loss coefficients. Similar observations were made when performing wake traverse measurements over a range of distances downstream of the cascades. At reduced distances, the measured loss coefficients ζ_{V2} approached those predicted (ζ_R).[1]

COMPARISON OF PROFILE LOSSES

Because the three cascades were manufactured to the same chord, surface lengths were quite dissimilar due to the very wide variation in deflection. Since the bulk of profile loss is known to originate from the suction-side, a Reynolds number based on the suction surface length (Res2) was defined.

Measured pressure loss coefficients (ζ_{V2}) versus gas deflection are plotted in Fig. 17 for three selected values of Res2. The general characteristic of loss falling with Re is due to the relation between friction loss and Re plus the reduced possibility of local separations. At Res2 = 10^6, the combination and mid-loaded cascades have transitional suction surface boundary layers close to the turbulent state. The aft-loaded profile demonstrates, at Res2 = 10^6, a less developed transitional boundary layer state and higher loss. Low base pressures indicate that this is due to the increase in effective trailing-edge loss.

At design conditions (Res2 = 4.10^5), a marked change in loss characteristic occurs due to the increased loss of the mid-loaded profile. This cascade is typified by a long suction-side diffusion which causes a laminar separation bubble at the trailing-edge. The loss difference between the forward and aft-loaded profiles is now duplicated. A small region of laminar detached flow at the aft-loaded profile's trailing-edge gives no marked increase in effective trailing-edge loss. This is because a laminar-like trailing-edge separation was already apparent at Res2 = 10^6.

For Res2 = 1.5 x 10^5, the shape of the loss curve changes because of greatly increased loss from the mid-loaded profile. For this profile, gross laminar separation causes very high form loss (i.e. trailing-edge loss with a much larger 'effective' trailing-edge thickness).

For the aft-loaded profile, lower losses are found because of the limited diffusion on the suction-side.

Because the combination-loaded profile imposes moderate suction-side diffusion, the design creates the least total blockage (with high base pressures) and reduced losses at low Re.

[1] The full conservation equations were applied, with the omission of tangential shear stress, turbulence and unsteady phenomena.

Downloaded from http://asmedigitalcollection.asme.org/GT/proceedings-pdf/GT1986/79283/V001T01A113/2396540/v001t01a113-86-gt-271.pdf by guest on 16 August 2022

CONCLUSIONS

A comparison of boundary layer data with profile losses has given greater understanding of the relevant profile loss mechanisms occurring in typical LP cascades. General conclusions to be drawn are:

i) For 'high' Re (10^6) and attached transitional suction-side boundary layers, the profile losses arise mainly from skin friction.

ii) At moderate Re (4×10^5), the transition point moves toward the trailing-edge. Although friction losses are reduced, the profile loss increases because 'effective' trailing-edge losses become important.

iii) At low Re (1×10^5), very high profile losses originate not only from friction but, of greater significance, from drag-generated trailing-edge losses, which become dominant.

It was found that the aft-loaded profile seriously delayed transition, even at high Re, and generated high profile loss.

The combination-loaded profile generated the lowest profile losses over the entire range of Re tested. Its good performance at low Re is due to the mild diffusion in the trailing-edge region.

The mid-loaded profile showed a rapid increase in profile loss with reducing Re, surpassing that of the aft-loaded profile by some 5% at $Res2 = 1.5 \times 10^5$. This was due to extensive laminar separation causing very high 'effective' trailing-edge loss.

Profile loss levels are all largely affected by suction-surface design. Traditional LP aerofoils operating at low Re will generate less profile loss if the design allows for a short region of transitional boundary layer in the trailing-edge region. This helps to minimise large 'effective' trailing-edge losses.

Extensive and high levels of suction-surface diffusion should be avoided on LP aerofoils required to operate at low Re.

ACKNOWLEDGEMENT

The authors wish to thank Rolls-Royce Limited and DFVLR for permission to publish this paper. The work has been carried out with the support of the Procurement Executive, Ministry of Defence.

The comments and conclusions are the opinions of the authors, which are not necessarily those of Rolls-Royce and DFVLR.

REFERENCES

1. Sharma, O.P., Wells, R.A., Schlinker, R.H., Bailey, D.A. Boundary Layer Development on Turbine Airfoil Suction Surfaces. ASME 81-GT-204 (1981).

2. Roberts, W.B. The Effect of Reynolds Number and Laminar Separation on Axial Cascade Performance. ASME Paper 74-GT-68 (1974).

3. Hebbel, H.H. Uber den Einfluss der Machzahl und der Reynoldszahl auf die Aerodynamischen Beiwerte von Turbinenschaufelgittern bei verschidener Turbulenz der Strömung. DFVLR/Ph.D Thesis (1962).

4. Hoheisel, H. and Kiock, R. Zwanzig Jahre Hochgeschwindigkeits-Gitterwindkanal des Instituts für Aerodynamik der DFVLR Braunschweig, Zeitschr. Flugwiss. Weltraumforsch. Vol. 1 (1977), pp. 17-29.

5. Hoeger, M. and Hoheisel, H. On the accuracy of boundary layer measurements in cascades at high subsonic speeds. 7th Symposium on measuring techniques for transonic and supersonic flow in cascades and turbomachines. Aachen (1983). Mitt. 1/84 Inst. Strahlantriebe RWTH Aachen (1984).

6. Kiock, R. Aus Wertung von Grenzschichtmessungen in Zweidimensionaler Kompressibler Strömung mit Druckgradient in der Grenzschicht. DFVLR Note 82-12 (1982).

7. Hodson, H.P. The Detection of Boundary-Layer Transition and Separation in High Speed Turbine Cascades. Proc. of the 7th Symposium on Measuring Techniques for Transonic and Supersonic Flow in Cascades and Turbomachines. 21-23 Sept. 1983, Aachen.

8. Klein, A. Aerodynamics of Cascades. Translated and revised from the original German "Aerodynamik der Schaufelgitter" by Prof. Dr.-Ing. N. Scholz. AGARD-AG-220 (1977).

9. Paterson, R.W., Weingold, H.D. "Experimental Investigation of a Simulated Compressor Airfoil Trailing-Edge Flowfield." AIAA Paper No. 84-0101 (1984).

10. Cebeci, T. and Smith, A.M.O. "Analysis of Turbulent Boundary-Layers." Academic Press (1974).

11. Denton, J.D. "A Survey and Comparison of Methods of Predicting The Profile Losses of Turbine Blades." CEGB Report RD/M/R147 (1971).

Downloaded from http://asmedigitalcollection.asme.org/GT/proceedings-pdf/GT1986/79283/V001T01A113/2396540/v001t01a113-86-gt-271.pdf by guest on 16 August 2022

APPENDIX

SUBSONIC AEROFOIL DESIGN CHARACTERISTICS

The PVD Diagrams (Fig. 2) are representative of the circulation (Γ) round each design. After Mach no. input data has been converted to Crocco no. (Q), the closed area of the transformed PVD diagram is given as:

$$a_o \oint Q\,ds^* = a_o \left[S_{os} \int_o^{'} Q_s\,ds^* - S_{op} \int_o^{'} Q_p\,ds^* \right]$$

$$= \oint U\,ds^* = \Gamma \qquad (1)$$

for adiabatic flow.

Therefore,

$$a_o \left[S_{os} \int_o^{'} Q_s\,ds^* - S_{op} \int_o^{'} Q_p\,ds^* \right] = s\Delta U_{w12} \qquad (2)$$

Both S_{os} and S_{op} are such that the axial chord is approximately common for any one design, i.e.

$$S_o/C_{ax} = K.$$

Thus

$$K_s a_o \int_o^{'} Q_s\,ds^* - K_p a_o \int_o^{'} Q_p\,ds^* = s/C_{ax}.\Delta U_{w12} \qquad (3)$$

The RHS of Eq. (3) is a form of lift coefficient which effectively fixes the net area of the PVD diagram. A family of aerofoils with similar maximum thickness/chord ratio will normally show K_s increasing at a greater rate than K_p as deflection rises, due to certain aerodynamic limitations on the design. These are:

i) Sub-sonic velocities

ii) Acceptable levels of adverse pressure gradient

iii) Acceptable regions of adverse pressure gradient

All are easily met when there is little restriction on s/Cax. Under these special circumstances, a variety of pressure distributions are possible for any value of ΔU_{w12}. However, there are normally strict mechanical limitations on aerofoil design which constrain s/Cax. These are minimum profile bulk and trailing-edge thickness. These must be achieved such that the resulting streamlined profile produces minimal form loss. Profile thickness tends to increase with deflection as the suction surface length and curvature rises to form a nominally contracting channel. This can be alleviated to some extent by incorporating pressure surface diffusion but, as deflection increases, limits ii) and iii) may eventually be exceeded. Cax - or thickness - may be scaled to suit an optimum lift coefficient by careful selection of the total number of aerofoils (i.e. s/Cax) as implied by Eq. (3). This also infers that where the above limitations are observed, s/Cax will tend to fall with deflection. Since this implies an increase in the number of aerofoils employed, lift-coefficients must be maximised if excessive turbine weight/disc stresses are to be avoided.

When the above optimisation is observed, it is found that the peak suction-surface Mach number generally moves aft with deflection (Fig. 18).[2]

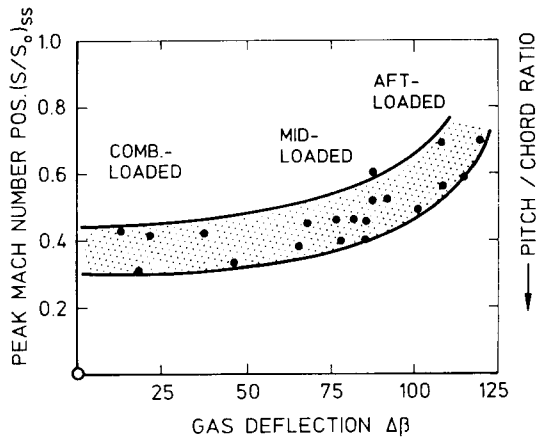

FIG.18 PEAK MACH NO. POSITION OF TYPICAL L.P. PROFILES.

T9, T10 and T11 were designed with these limits while optimising maximum thickness. The PVD designs are nevertheless representative of the characteristic loading and pressure distributions of low, medium and high deflection blading used in current sub-sonic LP turbines. The results and conclusions drawn from these tests are therefore pertinent to all sub-sonic LP profile designs.

[2] Sub-sonic LP blade, vane and cascade data from various sources. A similar effect is observed on turbine vanes and rotors where s/Cax varies radially with low hub/tip radius ratio.

Downloaded from http://asmedigitalcollection.asme.org/GT/proceedings-pdf/GT1986/79283/V001T01A113/2396540/v001t01a113-86-gt-271.pdf by guest on 16 August 2022